Published in final edited form as:
Inorg Chem. 2007 December 24; 46(26): 10981–10989. doi:10.1021/ic0701460.

A Pyrazolate-Supported $Fe_3(\mu_3\text{-}O)$-Core; Structural, Spectroscopic, Electrochemical and Magnetic Study

Dalice Piñero[a], **Peter Baran**[a,†], **Roman Boca**[b,d], **Radovan Herchel**[c,d*], **Michael Klein**[e], **Raphael G. Raptis**[a*], **Franz Renz**[e], and **Yiannis Sanakis**[f*]

a*Department of Chemistry and the Institute of Functional Nanomaterials, University of Puerto Rico, San Juan, PR 00931-3346*

b*Department of Inorganic Chemistry, Slovak University of Technology, SK-812 37 Bratislava, Slovakia*

c*Department of Chemistry, University of SS. Cyril and Methodius, Trnava, SK-91701, Slovakia*

d*Department of Inorganic Chemistry, Palacký University, Křížkovského 10, CZ-77147 Olomouc, Czech Republic*

e*Institute of Inorganic and Analytical Chemistry, Johannes Gutenberg-University, D-55099 Mainz, Germany*

f*Institute of Materials Science, NCRS "Demokritos", 15310 Aghia Paraskevi, Athens, Greece.*

Synopsis

A comparison is made between the structural, spectroscopic and magnetic properties of pyrazolate versus carboxylate complexes containing the $Fe_3(\mu_3\text{-}O)$-motif.

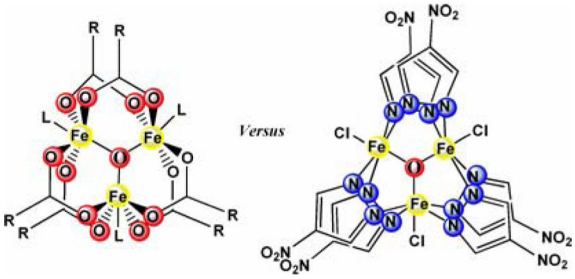

Introduction

Carboxylates constitute one of the widest families of transition-metal complexes and have been associated with numerous studies in all aspects of coordination chemistry. Their ubiquitous presence in Nature makes them an essential ligand in bioinorganic chemistry and an obvious choice when a chelating or bridging ligand is required. Since some early investigations of metal-metal interactions and magnetic exchange,[1] carboxylate complexes have an uninterrupted history as well in what has now become known as materials chemistry. In recent years, elegant studies of electron transfer and ground-breaking work in the new field of single molecule magnets have been carried out using transition metal carboxylates.[2,3]

*To whom correspondence should be addressed. E-mail: raphael@adam.uprr.pr (RGR), radovan.herchel@upol.cz (RH), sanakis@ims.demokritos.gr (YS).
†Present address: Department of Chemistry, Juniata College, Huntingdon, PA 16652.

In the course of our investigations of transition-metal pyrazolate chemistry, we became aware of the existence of a structural parallel between carboxylate and pyrazolate complexes of the same nuclearity: quite similar Pd-Pd distances are found in the trinuclear $[Pd(\mu\text{-}O_2CR)_2]_3$ and $[Pd(\mu\text{-}pz)_2]_3$ complexes (pz = pyrazolato, $C_3H_3N_2^-$, or substituted pyrazolato anion).[4,5] Additional examples exist in the literature, as between the tetranuclear Cu^I-carboxylates $[Cu(\mu\text{-}O_2CPh)]_4$ and $[Cu(\mu\text{-}O_2CCF_3)]_4$ on one hand and the pyrazolate $[Cu(\mu\text{-}3,5\text{-}Ph_2\text{-}pz)]_4$ on the other.[6,7] Replacement of one ligand by another, while the metal-core motif remains mostly unperturbed, can have significant effects on the physical properties of the metal centers, as both their electronic structure, as well as their electronic and magnetic communication are influenced by the donor-acceptor properties and orbital symmetry of the ligands. Perlepes et al. have shown that substitution of a hydroxide or cyanide by an azide bridge inverts the sign of magnetic exchange in nonanuclear Ni^{2+}, Co^{2+} and Fe^{2+} clusters.[8] Considering the central role of carboxylates as ligands in Coordination and Materials Chemistry -- particularly in the fast expanding field of single-molecule magnets [3] -- the development of a parallel class of structurally related pyrazolates would open-up a number of new possibilities. In order to investigate further this structural parallel and its accompanying effects, we turned our attention to one of the best known motifs in carboxylate chemistry, namely the $M_3(\mu_3\text{-}O)$- core, which includes examples of most transition metals.[9]

A variety of $[Fe_3(\mu_3\text{-}O)(\mu\text{-}O_2CR)_6L_3]$ complexes have been studied with regard to the magnetic and electronic interactions of their three paramagnetic metal centers.[10] The long metal-metal distances within the $Fe_3(\mu_3\text{-}O)$-unit preclude direct metal-metal bonding and the magnitude of the O-mediated antiferromagnetic exchange among them is determined by the Fe-O bond lengths.[11] Trinuclear $[Fe_3(\mu_3\text{-}O)(\mu\text{-}O_2CR)_6L_3]$ complexes have proven excellent starting materials for the synthesis of higher nuclearity clusters, taking advantage of the lability of carboxylate ligands.[12]

Here we report on the synthesis, characterization, X-ray crystal structure, infrared and electrochemical study of the trinuclear anion $[Fe_3(\mu_3\text{-}O)(\mu\text{-}4\text{-}O_2N\text{-}pz)_6Cl_3]^{2-}$ (**1**), (Figure 1), as its Et_3NH^+ (**a**), Bu_4N^+ (**b**) or PPh_4^+ (**c**) salts, along with the Electron Paramagnetic Resonance (EPR), the Mössbauer spectroscopy, magnetic susceptibility and magnetization studies for **1a**. We present a comparison among the best studied $[Fe_3(\mu_3\text{-}O)(\mu\text{-}LL)_6L_3]$ complexes with LL = carboxylate on one hand and the analogous LL = pyrazolate complexes reported here on the other, in order to better elucidate the relationship between the physical properties and the structural environment of the Fe_3O-motif.

Experimental Section

Synthesis

Reagents were purchased from Sigma-Aldrich and used without further purification. The anhydrous Fe^{III} salts were stored in a glove box compartment under argon. The ligand 4-O_2N-pzH was synthesized according to a literature method.[13] Infrared, ^1H NMR, and UV-vis spectra were recorded on a Nicolet FT-IR 6000, Bruker ADVANCE DRX-500, and Varian CARY 500 Scan, respectively.

$(Et_3NH)_4[Fe_3(\mu_3\text{-}O)(\mu\text{-}4\text{-}NO_2\text{-}pz)_6Cl_3]Cl_2$, 1a—A flask is charged with 0.750 g (4.62 mmol) anhydrous $FeCl_3$, 30 ml CH_2Cl_2 and 1.569 g (13.87 mmol) of 4-O_2N-pzH under an argon atmosphere, forming a partially soluble yellow solid. Dropwise addition of NEt_3 (1.611 ml, 11.5 mmol) to the reaction mixture under air, changes the solution color to dark red. X-ray quality single crystals were obtained by slow Et_2O vapor diffusion into the CH_2Cl_2 solution; yield, 52%, m.p. = 192 °C. Elemental analysis, found (calc.) for **1a**: C 34.82 (34.98), H 5.21 (5.31), N 21.23 (21.37); UV/Vis (CH_2Cl_2): λ_{max} = 291 nm; IR (KBr disk, cm^{-1}): ν = 1489 (s), 1407 (s), 1279 (s), 1163 (s), 1035 (s), 1008 (s), 976 (m), 888 (m), 837 (w), 815 (s), 759 (s),

682 (w), 626 (s), 600 (s), 551 (m), 476 (s); ^{1}H-NMR ($CDCl_3$) 30.87 ppm. The sample of **1a** used for magnetic susceptibility measurements was prepared from 99.99% $FeCl_3$.

$(Bu_4N)_2[Fe_3(\mu_3\text{-}O)(\mu\text{-}4\text{-}NO_2\text{-}pz)_6Cl_3]\cdot 0.5MeOH\cdot H_2O$, 1b—Complex **1b** is prepared similarly to **1a** in thf solvent, using a 1M Bu_4NOH/MeOH solution instead of NEt_3. X-ray quality single crystals are obtained by slow Et_2O vapor diffusion into a CH_2Cl_2 solution of the dark red reaction product; yield >20%, mp = 245 °C. Elemental analysis, found (calc.) for **1b**: C 41.29 (40.94), H 5.84 (5.99), N 19.13 (18.92).

$(Ph_4P)_2[Fe_3(\mu_3\text{-}O)(\mu\text{-}4\text{-}NO_2\text{-}pz)_6Cl_3]$, 1c—A flask is charged with 0.189g (0.35 mmol) $[Ph_4P][FeCl_4]$, 15 ml CH_2Cl_2 and 0.132 g (1.17 mmol) 4-O_2N-pzH. Drop wise addition of NEt_3 (0.162 ml, 1.16 mmol) turns the mixture to a dark red solution. X-ray quality single crystals were obtained by slow Et_2O diffusion into the CH_2Cl_2 solution; yield > 40%. m.p. = 277°C. Elemental analysis, found (calc.) for **1c**: C 48.63 (49.02), H 3.69 (3.64), N 14.51 (14.70).

X-Ray Crystallography

X-ray diffraction data, taken from a single crystal mounted atop a glass fiber with a Siemens SMART-CCD diffractometer (298 K, λ = 0.71073 Å), were collected on a Bruker AXS SMART 1K CCD, area detector with graphite monochromated Mo-Kα radiation (λ = 0.71073 Å) at room temperature using the program SMART-NT[14] and processed by SAINT-NT.[15] An empirical absorption correction was applied by the program SADABS. The structures were solved by direct method and refined by full-matrix least-squares methods on F^2.[16] All non-hydrogen atoms were refined anisotropically, while H-atoms were placed in calculated positions with their thermal parameters riding on those of their C-atoms. Crystallographic details for **1a**, **1b** and **1c** are summarized in Table 1.

Electrochemical experiments were performed with a BAS CV 50-W Voltammetric Analyzer, using non-aqueous $Ag/AgNO_3$ reference electrode for which the ferrrocene/ferricinium couple occurs at 0.200 V, Pt auxiliary electrode, and Pt working electrode. Magnetic functions were measured with a SQUID apparatus (Quantum Design) at B = 0.1 T from 2.0 to 300 K and the isothermal magnetization at T = 1.8 and 4.5 K, respectively. A correction to the underlying diamagnetism was estimated on the basis of Pascal constants as $\lambda_{dia} = -9.91\ 10^{-9}\ m^3\ mol^{-1}$ for **1a**. X-band EPR measurements were performed with powdered samples or acetone solutions of **1a** with a Bruker ER 200D instrument equipped with an ESR-9 Oxford cryostat and an Anristsu microwave frequency counter. Mössbauer measurements were recorded on a constant acceleration conventional spectrometer with a ^{57}Co (Rh matrix) source. Variable-temperature spectra were obtained by using Oxford cryostats, operating at 4.2 – 300 K. Isomer shift values (δ) are quoted relative to iron foil at 293 K.

Results and Discussion

The reactions of $FeCl_3$, (or PPh_4FeCl_4) with excess 4-O_2N-pzH and base (NEt_3, or Bu_4NOH) give the corresponding salts of **1**, which are recrystallized from CH_2Cl_2/Et_2O yielding analytically pure samples. A ~50% excess of pyrazole in the reaction mixture improves the crystalline product yield. The X-ray crystallographic analyses show that the all three dianions **1** contain six-coordinate Fe^{III}-centers forming an $Fe_3(\mu_3\text{-}O)$-core, supported by six bridging pyrazolates and three terminal chlorides (Fig. 1). Table 2 summarizes important bond lengths and angles for **1a–c**, respectively. While the molecular symmetry of anion **1** is $\boldsymbol{D}_{3h}$, consistent with the presence of a single resonance for all 12 protons in the ^{1}H-NMR/CDCl^3 spectrum, its crystallographic symmetry is two fold (**1a**), or lower (**1b,c**): Complex **1a** crystallizes on two-fold axis running along an Fe-O bond, with one short (3.269(1) Å) and two long (3.287(1) Å) Fe•••Fe distances. Whole trinuclear complex dianions are present in the asymmetric units of

1b and **1c**. The trinuclear complex dianion **1** packs efficiently with two PPh_4^+ counter ions in the crystal lattice, while the lattices of the Bu_4N^+ salt **1b** include interstitial solvent molecules. When the smaller NEt_3H^+ counter ion is employed, the crystal lattice of **1a** includes two interstitial $[NEt_3H]Cl$, besides the Fe_3-dianion. Inspection of packing diagrams shows that the shortest intermolecular contact in **1a** is an O•••O distance of 2.951 Å between two NO_2-groups, while the shortest intermolecular Fe•••Fe approach is of 7.995 Å. Similarly, the shortest intermolecular contacts, also between NO_2-groups, are O•••O of 3.301 Å in **1b** and 2.949 Å in **1c**, while the shortest intermolecular Fe•••Fe contacts for **1b** and **1c** are 9.882 and 10.307 Å, respectively.

The Fe-O and Fe•••Fe distances of **1** (Table 2) fall within the narrow ranges of the corresponding distances reported for analogous $Fe_3(\mu_3\text{-O})$-complexes of carboxylate or oxime ligands – 1.855 to 1.944 and 3.251 to 3.327 Å, respectively (Table 3).[10] Similarly, the infrared ν_{as}(Fe-O) bands for **1** occur at 626 cm^{-1} (598 cm^{-1} for ν_{as}(Fe-^{18}O)), also comparable to those reported for carboxylate analogues, 595 – 635 cm^{-1} (Table 4).[10 d, i–j]

Cyclic voltammetric analysis of **1b** (Fig. 2) in the +1.000 to −1.440 V window shows one reversible reduction at $E_{1/2}$ = −0.703 V (vs. Fc^+/Fc), followed by an irreversible one at − 1.246 V, which remains irreversible at 218 K. The voltammetric results are consistent with earlier studies of $Fe_3(\mu_3\text{-O})$-carboxylates showing a strongly ligand-dependent reversible reduction to the formally mixed-valent $Fe^{III}_2Fe^{II}$ species at $E_{1/2}$ values between −0.09 and −0.76 V.[10c] The $E_{1/2}$-values of the pyrazolate complex $[Fe_3(\mu_3\text{-O})(\mu\text{-}O_2Npz))_6Cl_3]^{2-}$ **1b** are shifted negative compared to those of the isovalent carboxylates $[Fe_3(\mu_3\text{-O})(\mu\text{-}O_2CR)_6L_3]^+$. This is largely due to the charge difference between the dianionic **1** (with three terminal chlorides) and the monocationic carboxylate complexes (with three neutral terminal ligands, L).

Mössbauer spectra from powdered samples of **1a** were recorded in the 4.2-300 K temperature range and zero external magnetic fields. Representative spectra are shown in Figure 3. At T > 20–30K the spectra comprise one relative symmetric quadrupole doublet with δ = 0.43 (1) mms^{-1} and ΔE_Q = 1.02(2) mms^{-1} at 78 K. No noticeable dependence of ΔE_Q on temperature is observed. On the other hand, the isomer shift decreases as the temperature increases (δ = 0.32(1) mms^{-1}, at 293 K). The temperature dependence of the isomer shift is attributed to the second-order Doppler effect.[17] The value of isomer shift in the whole temperature range is consistent with high spin ferric ions in N/O coordination environment. For temperatures below 20 K, an asymmetric line broadening is observed and is attributed to the onset of relaxation effects. Magnetic susceptibility studies (see below) indicate that the ground state of **1a** is characterized by *S* =1/2, which is the only thermally occupied state at liquid helium temperature. As the spin-lattice relaxation rate decreases at liquid helium temperatures, non-zero effective magnetic fields are induced at the iron nuclei, thus affecting the spectra.[18] Because the line broadening is larger for the lower energy line, a negative sign for the largest component of the Electron Field Gradient (EFG) tensor is inferred.[18] For complex **1a** the isomer shift fall at the lower end of the Fe^{III}_3O-carboxylate range (Table 5), indicating an increased degree of covalency for the present compounds compared to typical carboxylates.[10] On the other hand, the high quadrupole splitting value reflects the axial (locally C_{4v}) ClN_4O-coordination environment of the Fe-atoms of **1a**, compared to the pseudo-octahedral O_6-coordination of the carboxylate complexes listed in Table 5.

The overall temperature dependence of the effective magnetic moment for **1a** (Figure 4, Figure 5) indicates a sizable antiferromagnetic exchange. However, the low-temperature data reach a μ_{eff} value of 1.3 μ_B, lower than the theoretical limit of 1.7 μ_B for an *S* = 1/2 molecular spin predicted by isotropic exchange. In addition, the magnetization curve deviates progressively from the theoretical prediction when only the isotropic exchange is taken into account. The analysis of the magnetic susceptibility data (both χ *vs*. T and M *vs*. H) as well as the EPR spectra

(below), require the presence of non-Heisenberg interactions. These could be (a) single ion anisotropy, (zero field splitting D_i) (b) asymmetric (pseudodipolar) interaction D_{ij}, (c) antisymmetric interaction (d_{ij}).[19,20] With regard to the magnetic properties, the three terms induce the same effects, namely lowering of the g_{eff} for the $S = 1/2$ ground state and axial EPR signals with extremely low $g_\perp$ values. Consequently, the EPR results cannot be used as an argument for favoring one term over the other two. Rather, antisymmetric exchange (AE) is favored here on the basis of quantitative considerations based on the different effects that the terms (a), (b), and (c) have on the exchange coupling scheme of **1a**. Both D_i and D_{ij} mix states with higher S-values into the ground $S = 1/2$ state, inducing the aforementioned phenomena (low g_{eff} and $g_\perp$). Therefore, to a first approximation, the effects of these terms on the magnetic properties depend on the ratios D_i/J and D_{ij}/J respectively (J is the average value of the J_{ij}'s). The J_{ij} values can be accurately estimated from the fitting of the χ *vs.* T data. However, in order to achieve a good fitting of the magnetic data, unreasonably large D_i or D_{ij} values had to be assumed (because the magnitude of J leads to relatively large energy separation between the ground $S = 1/2$ states and the $S > 1/2$ states). Antisymmetric exchange, on the other hand, mixes the two $S = 1/2$ ground states; the effects on the magnetic properties of **1a** depend approximately on the ratio d_{ij}/δ, where δ is a measure of the non-equivalence between the J_{ij} values (lowering of the D_{3h} symmetry). As a result, the effects of AE are more pronounced for more symmetric triangles, where δ is close to zero and even a small value of d_{ij} can induce large anisotropies. Apart from the point-dipolar interaction (which has the same effects as the D_{ij} term) all the other terms arise from spin-orbit coupling, which is small (albeit non-zero) for Fe^{3+}(S=5/2) ions.

Therefore, a spin-Hamiltonian for an isosceles triangle with the isotropic, AE and molecular-field correction (Equation 1) has been postulated.

$$\widehat{H} = -J_1(\mathbf{S}_1\cdot\mathbf{S}_2+\mathbf{S}_2\cdot\mathbf{S}_3) - J_2(\mathbf{S}_1\cdot S_3)+\mathbf{d}_{12}\cdot(\mathbf{S}_1\times\mathbf{S}_2)+\mathbf{d}_{23}\cdot(\mathbf{S}_2\times\mathbf{S}_3)+\mathbf{d}_{31}\cdot(\mathbf{S}_3\times\mathbf{S}_1) + \mu_B B_a g(\widehat{S}_{1a}+\widehat{S}_{2a}+\widehat{S}_{3a}) - zj\langle\widehat{S}_a\rangle_T(\widehat{S}_{1a}+\widehat{S}_{2a}+\widehat{S}_{3a}) \quad (1)$$

where J_i are the isotropic exchange interaction parameters, $\mathbf{d}_{ij}$ are corresponding antisymmetric vectors, zj is a common molecular-field parameter, and $\langle S_a\rangle_T$ is a thermal average of the spin projection in the a-direction. For the magnetic field vector in the polar coordinates defined as $\vec{B}_a = B(\sin\theta\cos\varphi, \sin\theta\sin\varphi, \cos\theta)$ the molar magnetization was calculated as

$$M_{a,mol} = -N_A \frac{\sum_i \left(\sum_k\sum_l C^+_{ik}(Z_a)_{kl}C_{li}\right)\exp(-\varepsilon_{a,i}/KT)}{\sum_i \exp(-\varepsilon_{a,i}/KT)} \quad (2)$$

where Z_a is the matrix element of the Zeeman term for the a-direction of the magnetic field and C are the eigenvectors resulting from the diagonalization of the complete spin Hamiltonian matrix in local basis set of uncoupled kets (spin $S_i = 5/2$ for each center). Since a powder sample was used, the averaged molar magnetization was calculated as an orientational average using the *qromb* subroutine.[21]

$$M_{mol} = 1/4\pi\int_0^{2\pi}\int_0^{\pi} M_{a,mol}\sin\theta d\theta d\varphi \quad (3)$$

Since the averaged spin in Equation 1 needs eigenvectors, the equation has been solved by an iterative, time demanding procedure. The data were fitted simultaneously for the temperature-dependence and the field-dependence of the magnetization with the assumptions that: (a) The antisymmetric vector is equal for each pair, $\vec{d}_{12} = \vec{d}_{23} = \vec{d}_{31} = \vec{d}$ and only the z-component was assumed to be non-zero, $d_x = d_y = 0$. (b) The g-factors for Fe_{III} are fixed at $g_x = g_y = g_z = 2.0$. This leaves four free parameters, namely J_1, J_2, d_z and zj. Two different parameter sets were

found for **1a**, which is a common feature.[10n,22] First, for $J_1 > J_2$: J_1/hc = −80.1 cm^{-1}, J_2/hc = −72.4cm^{-1}, $|d_z|$/hc = 5.09 cm^{-1} and zj/hc = − 0.326 cm^{-1} (Figure 4) and second for $J_1 < J_2$: J_1/hc = −70.6 cm^{-1}, J_2/hc = −80.8 cm^{-1}, $|d_z|$/hc = 9.87 cm^{-1} and zj/hc = −0.325 cm^{-1} (Figure 5). The average values for the isotropic exchange are in both cases quite similar, J_{av}/hc = −77.5 cm^{-1} and J_{av}/hc = −74.0 cm^{-1}, respectively. The intermolecular interaction *zj* was found to be of antiferromagnetic nature and of the same value in both cases. The plots of the lowest energy levels for both parameter sets (S5) reveal that the ground state is $S = 1/2$ with effective *g*-factors $g_{\|,\mathrm{eff}} = 2.0$ and $g_{\perp\mathrm{eff}} = 0.84$ (for both fits). Such a low value for $g_{\perp\mathrm{eff}}$ is the result of the antisymmetric exchange.

The analyses of magnetic data for several analogous to **1** carboxylate complexes containing the $Fe_3(\mu_3\text{-}O)$-motif have yielded J-values in the range of −34.3 to −64.4 cm^{-1}, while a complex of a polydentate-N_5 ligand gave J/hc = −82.0 cm^{-1} (Table 6).[10b,f–h,l,n]

X-band EPR spectroscopy

From the analysis of the magnetic susceptibility data, an isolated S = 1/2 ground state was deduced for **1a**. The analysis also indicated the presence of AE interaction. Further evidence for the presence of AE comes from X-band EPR studies (Figure 6). In the absence of AE the $S = 1/2$ state is expected to be characterized by the intrinsic g_0- tensor of the transition metal ion. High spin ferric ions are characterized by a fairly isotropic intrinsic g_0-tensor. Therefore the EPR signal from the $S = 1/2$ ground state should consist of a symmetric derivative feature at $g_{\mathrm{eff}} \sim 2.0$. Indeed, such signals have been observed in the case of acetone solutions of $[Fe_3(\mu_3\text{-}O)(\mu\text{-}O_2CPh)_5(\mathrm{salox})L_1L_2]$ ($L_1 = L_2$ = MeOH or L_1 = EtOH, $L_2 = H_2O$, H_2salox= Salicylaldoxime).[10h] However, the EPR spectra of several trinuclear ferric complexes, either in the solid state or in solution, deviate significantly from this case. In general, the spectra comprise one relatively sharp peak at $g_{\mathrm{eff}} \sim 2.0$ and a broad tail at higher magnetic fields.[23] Such behavior is also found for Cr_3 and Cu_3 complexes.[24,25]

This characteristic EPR behavior has been successfully explained on the grounds of AE. Briefly, the AE term mixes the lowest two $S = 1/2$ states inducing an axial anisotropy in the *g*-tensor. The parallel component, $g_{\|}$, of the g-tensor lies along the direction of the antisymmetric pseudovector **d**, assumed perpendicularly to the triangle plane. Because the $g_{\|}$ component is not affected by the AE term, the EPR feature from this component consists of a rather sharp peak at a *g*-value, which coincides with the intrinsic g_0-tensor. The axial component, however, strongly depends on this parameter. To a first approximation, for a high spin triferric complex:[23a, 26]

$$g_{\perp} = g_0 \left[\frac{\delta^2 - (h\nu)^2}{\Delta^2 - (h\nu)^2} \right]^{1/2} \quad (4)$$

where $\Delta = \sqrt{\delta^2 + 243d^2}$, $h\nu$ is the energy of the microwave quantum (*ca*. 0.3 cm^{-1} at X-band) and g_0 the *g*-value of the intrinsic *g*-tensor of the high spin ferric ion (*ca*. 2.0). In this equation δ is the separation of the two lowest $S = 1/2$ doublets in the absence of AE. For a strictly equilateral configuration (all three isotropic exchange parameters, J_{ij}'s, equal) δ = 0. In this case the transition probability for an EPR signal at X-band vanishes.[23a] For a lower symmetry (i.e., isosceles configuration) $\delta \neq 0$ and then EPR transitions are possible. Therefore, observation of an EPR signal from the $S = 1/2$ ground state constitutes evidence for non-equivalent exchange coupling constants, J_{ij}'s.

From Equation 4, $g_{\perp}$ is expected to be lower than g_0 and indeed signals corresponding to $g_{\mathrm{eff}} \ll 2.0$ are observed in trinuclear complexes.[23] Inspection of Equation 4 indicates that $g_{\perp}$ is extremely sensitive in the parameters *d* and δ. This has the consequence that distributions

in these parameters induce large distribution in $g_{\perp}$. The broad high field tails observed in these systems have been attributed to such distributions.[23c,d, 26]

In Figure 6A, we show the EPR spectrum of a powdered sample of **1a** recorded at liquid helium temperatures. The spectrum exhibits a strong peak at g~2.0 superimposed on a broad signal. Careful inspection of the spectrum reveals also the presence of broad features at higher magnetic fields. These signals are shown in a different scale. The broad spectrum on which the sharp peak is superimposed is attributed to inter-molecular interactions present in the solid state. Such interactions have been considered in the analysis of the magnetic susceptibility data and have been observed in solid samples of other triferric complexes.[10h, 24e, 27]

In the present case, in order to minimize solid-state effects, we recorded a second EPR spectrum of **1a** dissolved in acetone (Figure 6B). The broad signal present in the solid sample is not observed in the acetone solution. Mononuclear high-spin ferric species usually give rise to characteristic signals at g~4.3. The weakness of the g~4.3 signal (which actually originates from impurities of the cavity) strongly suggests that no iron release in the form of high spin ferric mononuclear takes place upon dissolution. On the other hand, the sharp g~2.0 peak and the broad features at high magnetic fields are clearly retained in solution.

The EPR spectra of **1a**, either in the solid state or in solution, are attributed to the $S = 1/2$ ground state of the complex and are considered as evidence for the presence of AE interaction. Specifically, the sharp peak observed at g~2.0 is attributed to the $g_{\|}$ component. The broad features observed at higher fields are attributed to the $g_{\perp}$ part of the axial signal. As discussed earlier, only a lower than equilateral symmetry would lead to an EPR active ground state. Therefore, observation of these signals is in line with the analysis of the magnetic susceptibility data, which was based on an isosceles rather than on an equilateral configuration. Application of the analytical Equation 4 using the parameters of the exchange coupling constants and the magnitude of the antisymmetric parameter *d* derived from the magnetic susceptibility data, yield a value of *ca*. 0.57 for $g_{\perp}$. The EPR spectra at the high magnetic field region, however, do not exhibit a feature corresponding to a well-defined $g_{\perp}$ value. Instead, the broad high field signals indicate a rather broad distribution with $g_{\perp} < 1.1 - 1.2$, which is in reasonable agreement with the value ($g_{\perp, \text{eff}} = 0.84$) derived from the magnetization data. As discussed above, the distribution in $g_{\perp}$ are interpreted on the basis of distribution in J_{ij}'s and/or *d*. The slight line-shape differences observed in the high magnetic field signals in 5A and 5B may result from differences in the distribution profiles between solid and solution phases.

Evidence for the presence of AE is provided on the basis of magnetic susceptibility measurements and X-band EPR spectroscopy. Moreover, EPR spectroscopy suggests also distributions in J_{ij} and/or the parameter *d*. Such distributions are probably not discernible in the magnetic susceptibility measurements, which under the above discussion reflect a mean over an unknown distribution.

Conclusion

Complexes of formula $[Fe_3(\mu_3\text{-}O)(\mu\text{-}LL)_6L_3]$ have been described for a variety of bridging LL ligands, including carboxylate, oxime, linked-pyridine/tetrazole and now 4-nitropyrazole, as well. With regard to the $Fe_3(\mu_3\text{-}O)$-motif, both the Fe-O bond lengths and the Fe•••Fe separations of **1** are quite similar to those of the previously published structures (Table 3).[10] Comparison of the spectroscopic (IR, Mössbauer) data (*vide supra*) also indicates that the $Fe_3(\mu_3\text{-}O)$-motif is not significantly affected by the replacement of carboxylate by pyrazolate ligands, with the pyrazolate data resembling closer those of the benzoate.[10b,e,h] In contrast, the magnetic data differ significantly between the pyrazolate and carboxylate materials (Table 6) with the former having a larger antiferromagnetic exchange value than the latter. The value

of antiferromagnetic exchange constant of **1a** falls close to those predicted by the models of Gorun and Lippard on the basis of the Fe - O distances, as well as by that of Christou et al. on the basis of Fe – O distances and Fe – O – Fe angles.[11,28] Both models predict accurately J-values in polynuclear Fe^{III}-systems that involve negligible contribution by a secondary magnetic exchange pathway. The J-value predicted by the Gorun and Lippard relatioship for **1** is approximately $-70\ cm^{-1}$, while that of Christou *et al*. is $-69.7\ cm^{-1}$, both > 5% lower than the actual J-value determined here (average J-values of **1a** are $-77.5\ cm^{-1}$ and $-74.0\ cm^{-1}$). The latter are lower than the values calculated for and measured in $Fe_4(\mu_3\text{-}O)_2$ "butterfly"-type complexes by Ruiz *et al.*[29] and the dioxime complex $[Fe_3O(bamen)_3]^+$.[10g] While the principal magnetic exchange path, Fe-O-Fe (a two-bond path), is practically identical in the pyrazolate and carboxylate complexes discussed here, the corresponding contributions of the secondary 3-bond (pyrazolate) versus the 4-bond (carboxylate) paths are evidently different. Pyrazolates have been known for a long time as efficient mediators of antiferromagnetic exchange,[30] and an important contribution of μ-pyrazolato ligands has recently been invoked for the interpretation of magnetic exchange among Cu^{II}-centers.[31] As a result, the overall antiferromagnetic exchange increases in magnitude in the case of the pyrazolate complex **1a** compared to its analogous carboxylates. This is also consistent with the higher degree of covalency of **1a** compared to its carboxylate analogues revealed by Mössbauer spectroscopy. Consequently, polynuclear pyrazolato complexes of open-shell metals are expected to show different magnetic properties than those of the corresponding carboxylates. Apart from the magnitude of the isotropic exchange interaction, the present complexes are also characterized by significant antisymmetric exchange.

Supplementary Material

Refer to Web version on PubMed Central for supplementary material.

Acknowledgment

Financial support of this work at UPR was received from NIH-SCoRE-5S06GM08102. DP acknowledges GAANN (P200A030197-05) and RISE (2-R25-GM6-1151) doctoral scholarships. Financial support of the VEGA 1/2453/05 and APVT 20-005204 programs (RB and RH), Slovakia and MSM6198959218 (RH), Czech Republic, is acknowledged.

References

1. (a) Figgis BN, Robertson GB. Nature 1965;205:694. (b) Beckett R, Cotton R, Hoskins BF, Martin RL, Vince DG. Aust. J. Chem 1969;22:2527.
2. (a) Londergan CH, Salsman JC, Ronco S, Dolkas LM, Kubiak CP. J. Am. Chem. Soc 2002;124:6236. [PubMed: 12033841] (b) Londergan CH, Kubiak CP. J. Phys. Chem. A 2003;107:9301.
3. (a) Christou G, Gatteschi D, Hendrickson DN, Sessoli R. MRS Bulletin 2000:66.and references therein (b) Soler M, Wernsdorfer W, Folting K, Pink M, Christou G. J. Am. Chem. Soc 2004;126:2156. [PubMed: 14971951] (c) Mishra A, Wernsdorfer W, Abboud KA, Christou G. J. Am. Chem. Soc 2004;126:15648. [PubMed: 15571379] (d) Milios CJ, Vinslava A, Whittaker AG, Parsons S, Wernsdorfer W, Christou G, Perlepes SP, Brechin EK. Inorg. Chem 2006;45:5272. [PubMed: 16813386]
4. (a) Baran P, Marrero CM, Pérez S, Raptis RG. Chem. Commun 2002:1012. (b) Umakoshi K, Yamauchi Y, Nakamiya K, Kojima T, Yamasaki M, Kawano H, Onishi M. Inorg. Chem 2003;42:3907. [PubMed: 12793829]
5. (a) Smart ML, Skapski AC. J. Chem. Soc., Chem. Commun 1970:658. (b) Djalina NN, Dargina CV, Sobolev AN, Buslaeva TM, Romm IP. Koord. Khim 1993;19:57. (c) Bancroft DP, Cotton FA, Falvello LR, Shwotzer W. Polyhedron 1988;7:615. (d) Cotton FA, Han S. Rev. Chim. Miner 1985;22:277.
6. (a) Drew MGB, Edwards DA, Richards R. J. Chem. Soc., Dalton Trans 1977:299. (b) Cotton FA, Dikarev EV, Petrukhina MA. Inorg. Chem 2000;39:6072. [PubMed: 11151506] (c) Reger DL, Huff

MF, Wolfe TA, Adams RD. Organometallics 1989;8:848. (d) Rodesiler PF, Amma EL. Chem. Commun 1974:599.

7. Ardizzoia GA, Cenini S, LaMonica G, Masciocchi N, Maspero A, Moret M. Inorg. Chem 1998;37:4284. [PubMed: 11670564]
8. (a) Papaefstathiou GS, Escuer A, Vicente R, Font-Bardia M, Solans X, Perlepes SP. Chem. Commun 2001:2414. (b) Papaefstathiou GS, Perlepes SP, Escuer A, Vicente R, Font-Bardia M, Solans X. Angew. Chem. Int. Ed 2001;40:884. (c) Boudalis AK, Donnadieu B, Nastopoulos V, Clemente-Juan J-M, Mari A, Sanakis Y, Tuchagues J-P, Perlepes SP. Angew. Chem. Int. Ed 2004;43:2266.
9. Cannon RD, White RP. Prog. Inorg. Chem 1988;36:195.
10. (a) Blake AB, Fraser LR. J. Chem. Soc., Dalton Trans 1975:193. (b) Degang F, Guoxiong W, Wenxia T. Polyhedron 1993;12:2459. (c) Bond AM, Clark RJH, Humphrey DG, Panayiotopoulos P, Skelton BW, White AH. J. Chem. Soc., Dalton Trans 1998:1845. (d) Wu R, Pouraz M, Sowrey FE, Anson CE, Wocadlo S, Powell AK, Jayasooriya UA, Cannon RD, Nakamoto T, Katada M, Sano H. Inorg. Chem 1998;37:1913. (e) Sowrey FE, Tilford C, Wacadlo S, Anson CE, Powell AK, Bennington SM, Montfrooij W, Jayasooriya UA, Cannon RD. J. Chem. Soc., Dalton Trans 2001:862. (f) Hibbs P, van Koningsbruggen PJ, Arif AM, Shum WW, Miller JS. Inorg. Chem 2003;42:5645. [PubMed: 12950213] (g) Sreerama SG, Pal S. Eur. J. Inorg. Chem 2004:4718. (h) Raptopoulou CP, Sanakis Y, Boudalis AK, Psycharis V. Polyhedron 2005;24:711. (i) Johnson MK, Powell DB, Cannon RD. Spectrochim. Acta 1981;37A:995. (j) Montri L, Cannon RD. Spectrochim. Acta 1985;41A:643. (k) Dziobkowski CT, Wrobleski JT, Brown DB. Inorg. Chem 1981;20:671. (l) Gavrilenko KS, Addison A, Thompson L, Pavlishchuk VV. Theor. and Exp. Chem 2004;40:214. (m) Stadler C, Daub J, Köhler J, Saalfrank RW, Coropceanu V, Schünemann V, Ober C, Trautwein AX, Parker SF, Poyraz M, Inomata T, Cannon RD. J. Chem. Soc., Dalton Trans 2001:3373. (n) Boudalis AK, Sanakis Y, Dahan F, Hendrich M, Tuchagues J-P. Inorg Chem 2006;45:443. [PubMed: 16390088]
11. Gorun SM, Lippard SJ. Inorg. Chem 1991;30:1625.
12. (a) Yao H, Wang J, Ma Y, Waldmann O, Du W, Song Y, Li Y, Zheng L, Decurtins S, Xin X. Chem. Commun 2006:1745. (b) Benelli C, Parsons S, Solan GA, Winpenny REP. Angew. Chem. Int. Ed. Engl 1996;35:1825. (c) Taft M, Wernsdorfer W, Folting K, Pink M, Christou G. J. Am. Chem. Soc 2004;126:2156. [PubMed: 14971951]
13. Maresca KP, Rose DJ, Zubieta J. Inorg. Chim. Acta 1997;260:83.
14. SMART-NT. Version 5.0. Madison, WI: Brucker AXS; 1998.
15. SAINT-NT. Version 5/6.0. Madison, WI: Brucker AXS; 1999.
16. SHELXTL-NT. Version 5.1. Madison, WI: Brucker AXS; 1998.
17. Greenwood, NN.; Gibb, TC. Mössbauer Spectroscopy. London: Chapman and Hall Ltd; 1971.
18. Blume M. Phys. Rev. Lett 1965;14:96.
19. (a) Dzyaloshinski I. J. Phys. Chem. Solids 1958;4:241. (b) Moriya T. Phys. Rev 1960;120:91. (c) Tsukerblat BS, Belinskii MI, Fainzil'berg VE. Sov. Sci. Rev. B Chem 1987;9:337. (d) Bencini A, Gatteschi D. Mol. Phys 1982;47:161.
20. (a) Boca R. Coord. Chem. Rev 2004;284:757.Boca, R. Theoretical Foundations of Molecular Magnetism. Amsterdam: Elsevier; 1999. Bencini, A.; Gatteschi, D. EPR of Exchanged Coupled Systems. Berlin: Springer-Verlag; 1990.
21. Numerical recipes in Fortran. http://www.nr.com
22. Jones DH, Sams DH, Sams JR, Thompson RC. J. Chem. Phys 1984;81:440.
23. (a) Rakitin YV, Yablokov YV, Zelentsov VV. J. Magn. Reson 1981;43:288–301. (b) Caneschi A, Cornia A, Fabretti AC, Gatteschi D, Malavasi M. Inorg. Chem 1995;34:4660. (c) Sanakis Y, Boudalis AK, Tuchagues J-P. C. R. Chimie 2007;10:116.and references therein
24. (a) Yablokov YV, Gaponenko VA, Ablov AV, Zhkhareva TN. Sov. Phys. Solid State 1973;15:251. (b) Nishimura H, Date M. J. Phys. Soc. Jpn 1985;54:395. (c) Honda M, Morita M, Date M. J. Phys. Soc. Jpn 1992;61:3773. (d) Vlachos A, Psycharis V, Raptopoulou CP, Lalioti N, Sanakis Y, Diamantopoulos G, Fardis M, Karayanni M, Papavassiliou G, Terzis A. Inorg. Chim. Acta 2004;357:3162. (e) Psycharis V, Raptopoulou CP, Boudalis AK, Sanakis Y, Fardis M, Diamantopoulos G, Papavassiliou G. Eur. J. Inorg. Chem 2006;18:3710.
25. (a) Liu XM, de Miranda MP, McInnes EJL, Kilner CA, Halcrow MA. Dalton Trans 2004:59. [PubMed: 15356742] (b) Yoon J, Mirica LM, Stack TDP, Solomon EI. J. Am. Chem. Soc

2004;126:12586. [PubMed: 15453791] (c) Belinsky MI. Inorg. Chem 2004;43:739. [PubMed: 14731038] (d) Stamatatos TC, Vlahopoulou JC, Sanakis Y, Raptopoulou CP, Psycharis V, Boudalis AK, Perlepes SP. Inorg. Chem. Comm 2006;9:814.

26. Sanakis Y, Macedo AL, Moura I, Moura JJ, Papaefthymiou V, Münck E. J. Am. Chem. Soc 2000;122:11855.
27. Boudalis AK, Sanakis Y, Raptopoulou CP, Terzis A, Tuchagues J-P, Perlepes SP. Polyhedron 2005;24:1540.
28. Cañada-Vilalta C, O'Brien TA, Brechin EK, Pink M, Davidson ER, Christou G. Inorg. Chem 2004;43:5505. [PubMed: 15332801]
29. Cauchy T, Ruiz E, Alvarez S. J. Am. Chem. Soc 2006;128:15722. [PubMed: 17147382]
30. (a) Berends HP, Stephan DW. Inorg. Chem 1987;26:749. (b) Ehlert MK, Rettig SJ, Storr A, Thompson RC, Trotter J. Can. J. Chem 1989;76:1970.
31. Koval IA, van der Schilden K, Schuitema AM, Gamez P, Belle C, Pierre J-L, Lüken M, Krebs B, Roubeau O, Reedijk J. Inorg. Chem 2005;44:4372. [PubMed: 15934768]

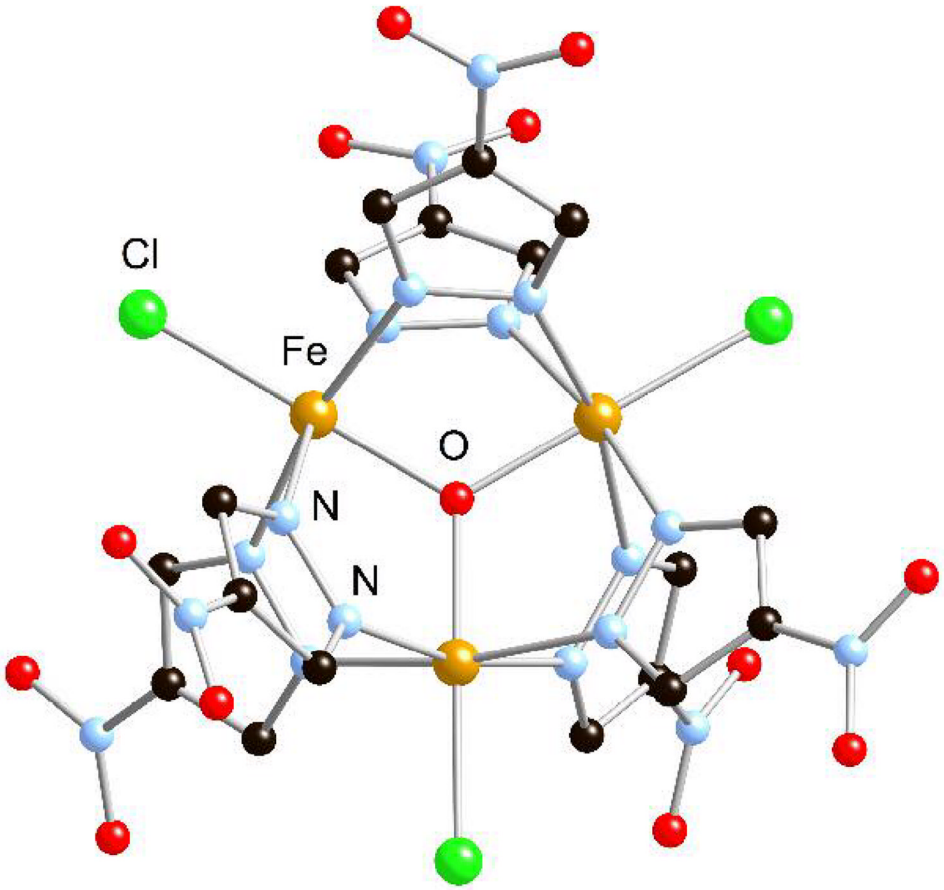

Figure 1.
Ball-and stick diagram of anions **1**.

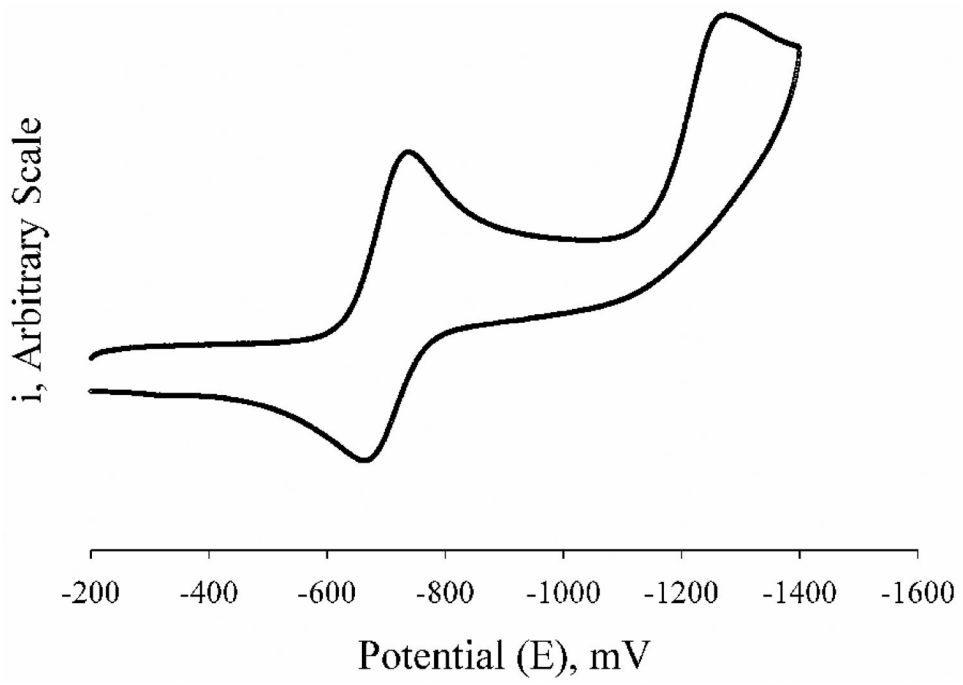

Figure 2.
Cyclic voltammogram (0.03M Bu_4NPF_6/CH_2Cl_2, 295 K, Pt-working electrode, $Ag/AgNO_3$ reference, 100 mV/s sweep) of **1b** from-200 mV to −1400 mV, vs Fc/Fc^+.

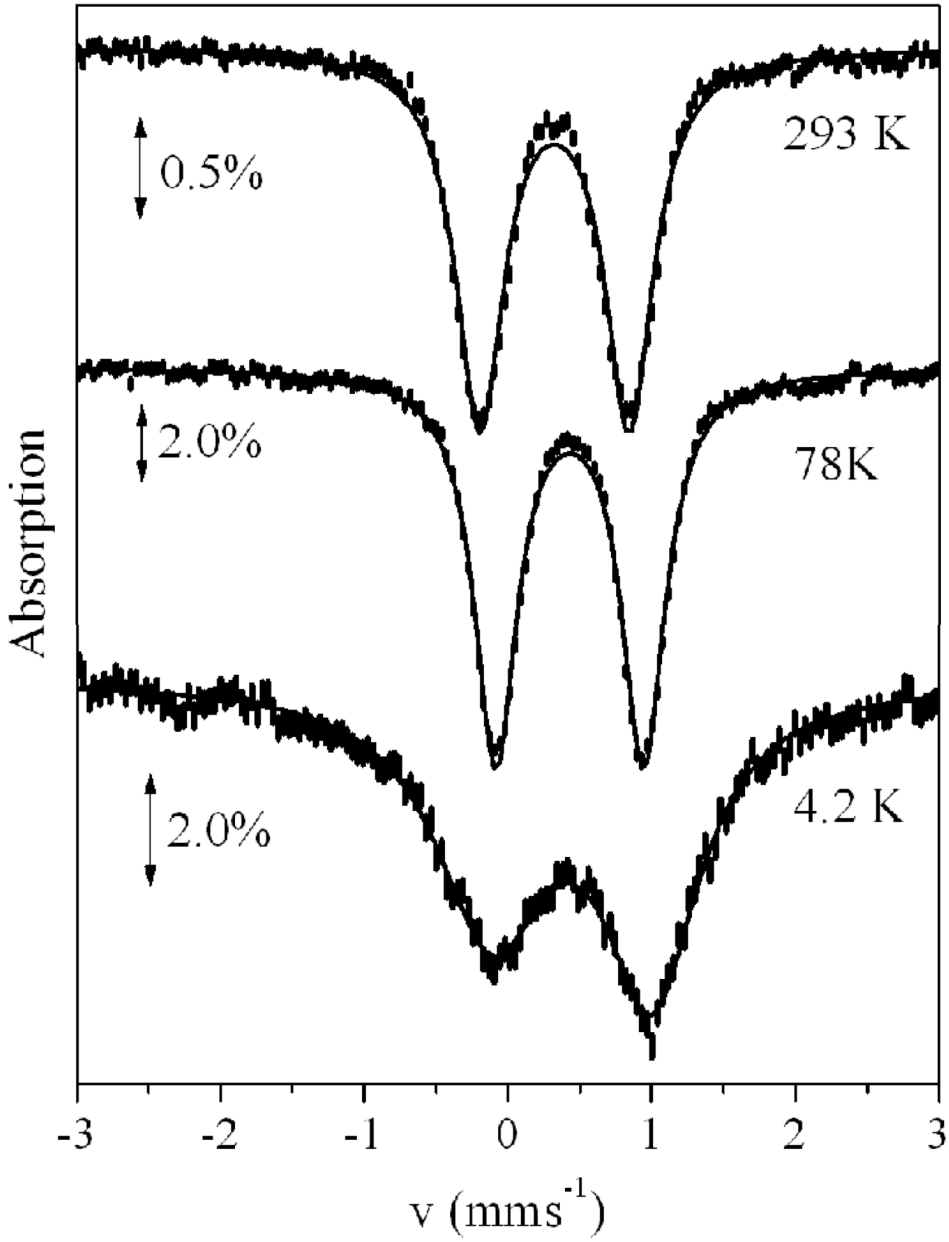

Figure 3.
Mössbauer spectra of **1a** at 293 K, 78 K and 4.2 K.

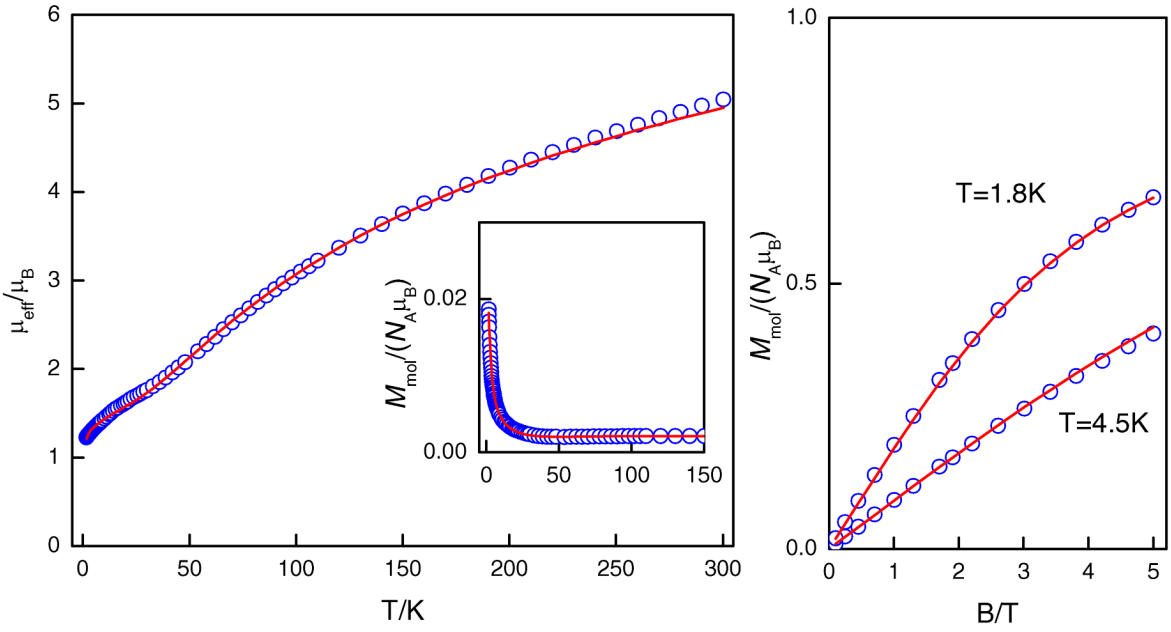

Figure 4.

Temperature dependence of the effective magnetic moment (left, $B = 0.1$ T) and magnetization (right, $T = 1.8$ and 4.5 K) for **1a**. Inset: Temperature dependence of the molar magnetization. Open circles, experimental data; red solid line – best-fit for $J_1/hc = -80$ 1 cm^{-1}, $J_2/hc = -72.4$ cm^{-1}, $|d_z|/hc = 5.09$ cm^{-1} and $zj/hc = -0.326$ cm^{-1}.

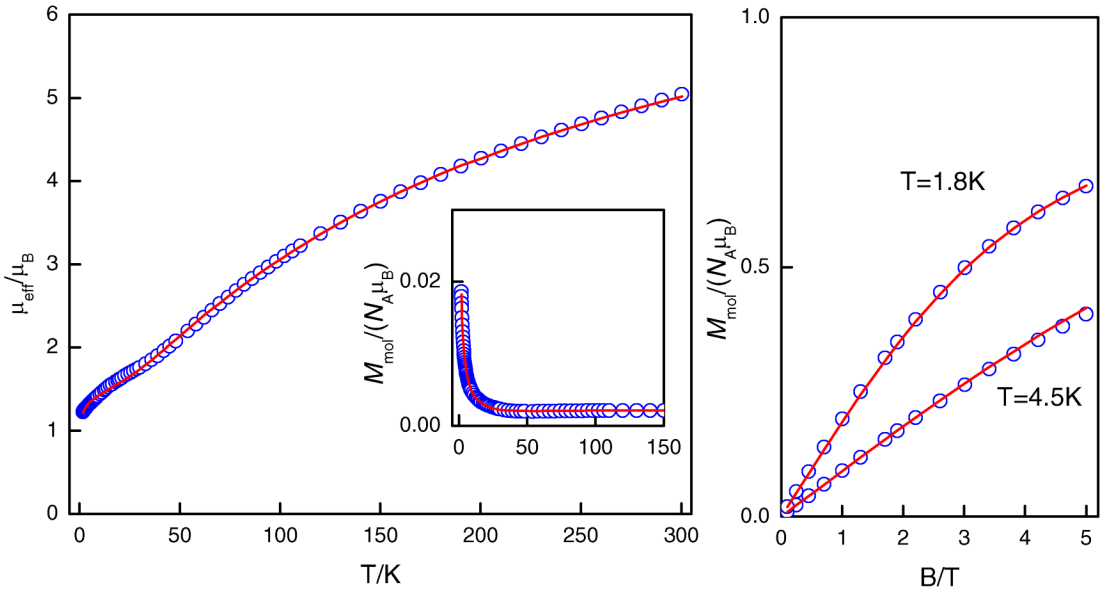

Figure 5.

Temperature dependence of the effective magnetic moment (left, $B = 0.1$ T) and magnetization (right, $T = 1.8$ and 4.5 K) for **1a**. Open circles, experimental data; solid line, best-fit for $J_1/hc = -70\ 6\ cm^{-1}$, $J_2/hc = 80\ 8\ cm^{-1}$, $|d_z|/hc = 9.87\ cm^{-1}$ and $zj/hc = -0.325\ cm^{-1}$.

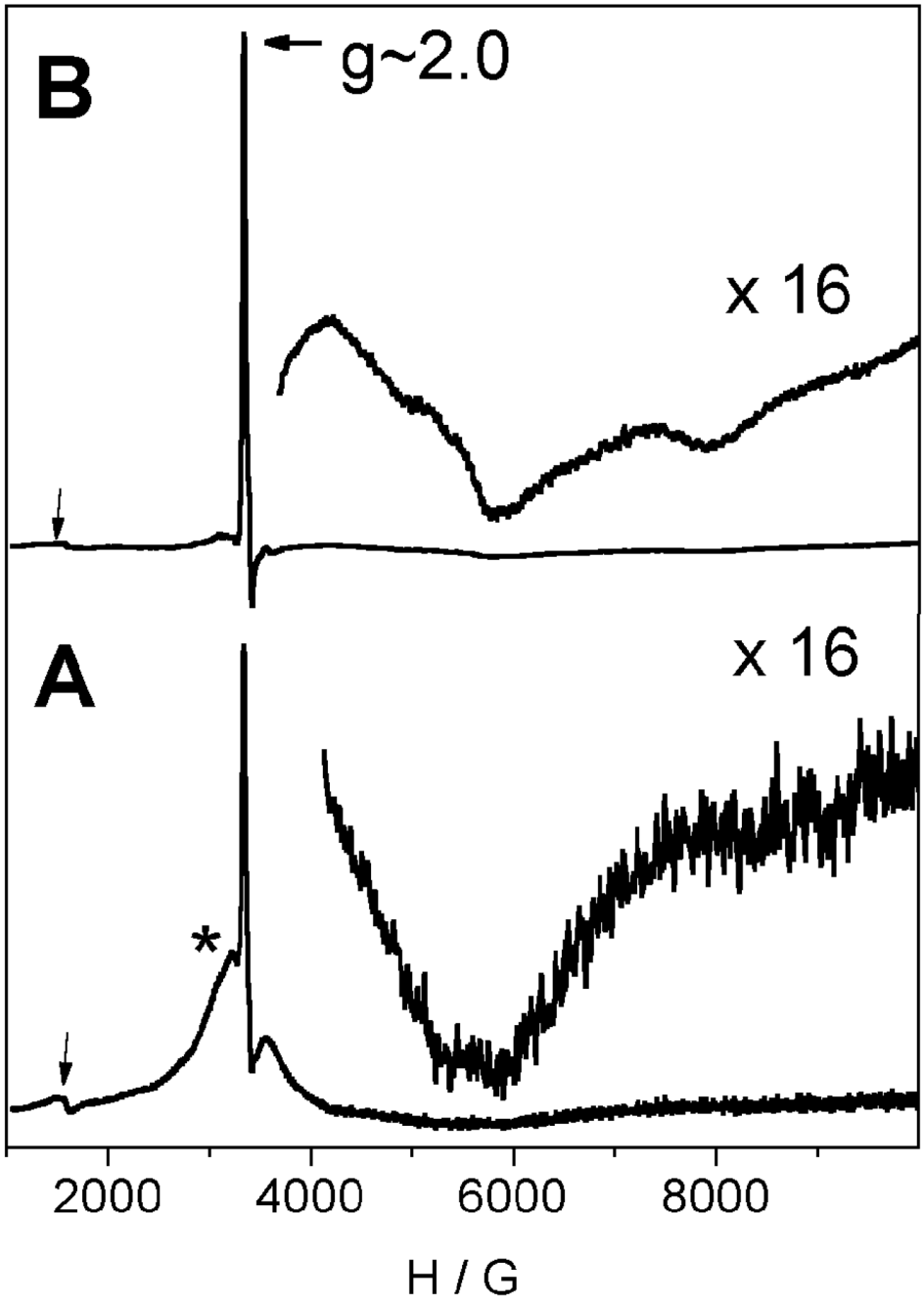

Figure 6.
X-band (9.4 GHz) EPR spectra from powdered sample of **1a** (A) and from an acetone glass (B). The vertical arrows indicate the g~4.3 signal attributed to ferric impurities. The asterisk in A indicates the broad signal at g~2.0 which is absent in B. EPR conditions: (A) Temperature, 4.2 K; microwave power, 10 mW; modulation amplitude 25 Gpp; (B) Temperature, 5.1 K, microwave power, 2 mW, modulation amplitude 25 G_{pp}.

Table 1

Crystallographic data for **1a, 1b** and **1c**.

	1a	1b	1c
Empirical formula	$C_{42}H_{76}Cl_5Fe_3N_{22}O_{13}$	$C_{50.5}H_{88}Cl_3Fe_3N_{20}O_{14.5}$	$C_{66}H_{52}Cl_3Fe_3N_{18}O_{13}P_2$
Fw	1442.05	1481.31	1641.10
Temp (K)	298	299	298(2)
Wavelength (Å)	0.71073	0.71073	0.71073
Cryst syst	Orthorhombic	Monoclinic	Monoclinic
Space group	*Pbcn*	$P2_1/c$	$P2_1/n$
***a*(Å)**	24.344(4)	17.811(3)	17.532(3)
***b*(Å)**	10.672(2)	15.399(2)	18.109(3)
***c*(Å)**	25.978(4)	26.573(4)	24.150(4)
β(deg)	90	101.809(3)	106.755(3)
***V*(Å)**	6748.7(2)	7134.0(2)	7342(2)
Z	4	4	4
Density (cal) (Mg m^{-3})	1.419	1.379	1.485
Abs coeff (mm^{-1})	0.904	0.785	0.811
Cryst size (mm)	0.14 × 0.10 × 0.10	0.29 × 0.22 × 0.15	0.16 × 0.14 × 0.14
Independent reflns/ I >2σ(I)	4852 / 3055	15937 / 9304	12952 / 6696
R / R_w	0.0497 / 01183	0.0677 / 0.1451	0.0472 / 0.0846
F(000)	2996	3104	3348
GoF	1.003	1.044	0.902

Table 2

Selected bond lengths (Å) and angles (deg) for **1a–c**.

	1a	**1b**	**1c**
	$C_{42}H_{76}Cl_5Fe_3N_{22}O_{13}$	$C_{50.5}H_{88}Cl_3Fe_3N_{20}O_{14.5}$	$C_{66}H_{52}Cl_3Fe_3N_{18}O_{13}P_2$
Fe…Fe	3.269(1), 3.287(1)	3.269(4) – 3.287(1)	3.265(1) – 3.292(2)
Fe-O	1.885(4), 1.894(2)	1.889(3) – 1.898(3)	1.878(2) – 1.904(2)
Fe-N	2.129(3) – 2.152(4)	2.116(3) – 2.161(4)	2.116(4) – 2.149(3)
Fe-X	2.280(2), 2.284(2)	2.272(1) – 2.294(1)	2.263(1) – 2.291(1)
Fe-O-Fe	120.4(1), 119.1(2)	120.6(1) – 119.4(1)	119.7(1) – 120.3(1)
O-Fe-X	177.7(1), 180.000(1)	177.63(9) – 178.98(9)	177.51(8) – 179.9(1)

Table 3

Fe-˜O and Fe•••Fe distances for selected $[Fe_3(\mu_3\text{-}O)(\mu\text{-}LL)_6X_3]$ complexes.

	Fe-O (Å)	Fe…Fe (Å)	Ref.
$[Fe_3O(O_2CCH_3)_6(isoxazole)_3]ClO_4$	1.901, 1.894	3.286, 3.284	10f
$[Fe_3O(O_2CPh)_6(CH_3OH)_3]NO_3$	1.890, 1.907	3.274, 3.300, 3.284	10b
$[Fe_3O(O_2CPh)_5(salox)(MeOH)_2]$	1.855, 1.882, 1.944	3.254, 3.251, 3.327	10h
$[Fe_3O(O_2CPh)_6(py)_3]NO_3$	1.9084	3.306	10c
$[Fe_3O(bamen)_3]^+$	1.898, 1.911	3.299, 3.301	10g
$[Fe_3O(piv)_6(MeOH)_3]^+$	1.905	3.274	10a
$[NaFe_3O(O_2CPh)_5(pic)_2(EtOH)_2(H_2O)]_2(ClO_4)_2$	1.897, 1.917, 1.933	3.283, 3.285, 3.371	10n

Table 4

Infrared $\nu_{(Fe\text{-}O)}$ stretches for selected $[Fe_3(\mu_3\text{-}O)(\mu\text{-}LL)_6X_3]$ complexes.

	$\nu_{as}(Fe_3O)$	Reference
1a	626 (^{18}O; 598)	this work
$[Fe_3O(O_2CH)_6(H_2O)_3]NO_3$	595	10i
$[Fe_3O(O_2CCH_3)_6(H_2O)_3]ClO_4$	609	10i
$[Fe_3O(O_2CCH_3)_6(py)_3]NO_3$	604	10i
$[Fe_3O(O_2CCH_3)_6(\gamma\text{-pic})]ClO_4$	605	10i
$[Fe_3O(O_2CCH_3)_6(py)_3][FeCl_4]$	600 (^{18}O; 580)	10j
$[Fe_3O(O_2CCH_3)_6(py)_3]ClO_4$	635	10d
$[Fe_3O(O_2CPh)_6(py)_3]ClO_4$	622	10e
$[Fe_3O(O_2CCH_3)_6(H_2O)_3]ClO_4$	520	10k

Table 5

Mössbauer isomer shift (δ) and quadrupole splitting (ΔE_Q) values for selected $[Fe_3(\mu_3\text{-}O)(\mu\text{-}LL)_6Cl_3]$ complexes.

	δ, mm s^{-1}	**ΔE_Q, mm s^{-1}**	**Reference**	
1a	0.43(1)	1.02(2)	This work,	T = 78 K
	0.32(1)	1.04(2)	This work,	T = 300K
$[Fe_3O(O_2CCH_3)_6(H_2O)_3]ClO_4$	0.53	0.74	10k, T = 21 K	
	0.42	0.58		T = 295 K
$[Fe_3O(O_2CCH_2CO_2)_3(H_2O)_3]ClO_4$	0.52	0.72	10k, T = 21 K	
	0.41	0.58		T = 295 K
$[Fe_3O(O_2CCH_2CH_2CO_2)_3(H_2O)_3]ClO_4$	0.53	0.81	10k, T = 22 K	
	0.42	0.67		T = 295 K
$[Fe_3O(O_2CCHCHCO_2)_3(H_2O)_3]ClO_4$	0.51	0.88	10k, T = 20 K	
	0.42	0.79		T = 295 K
$[Fe_3O(o\text{-phthalate})_3(H_2O)_3](o\text{-phthalate})_{0.5}$	0.52	0.82	10k, T = 22K	
	0.41	0.81		T = 295 K
$[Fe_3O(m\text{-phthalate})_3(H_2O)_3(m\text{-phthalate})$	0.53	0.93	10k, T = 22 K	
	0.42	0.79		T = 295 K
$[Fe_3O(ditetrazole)_3]NO_3$	0.44	1.10	10m, T = 4.2 K	
$[Fe_3O(O_2CPh)_6(CH_3OH)_3]NO_3$	0.31	0.346	10b,	T = room temp.
$[NaFe_3O(O_2CPh)_5(pic)_2(EtOH)_2(H_2O)]_2(ClO_4)_2$	0.51	0.70	10n, T = 78 K	
	0.40	0.59		T = 298 K

Table 6

Magnetic exchange coupling constants* for selected $[Fe_3(\mu_3\text{-}O)(\mu\text{-}LL)_6X_3]$ complexes.

	J/hc, cm^{-1}	Reference
1a	−80.1, −72.4	
	−70.6, −80.8	This work
$[Fe_3O(O_2CCH_3)_6(isoxazole)_3]ClO_4$	−58.8, −34.3	10f
$[Fe_3O(O_2CPh)_6(CH_3OH)_3]NO_3$	−54.12	10b
$[Fe_3O(O_2CPh)_5(salox)(MeOH)_2]$	−54.6	10h
$[Fe_3O(bamen)_3]^+$	−82.0	10g
$[Fe_3O(O_2CCH_3)_6(pyz)_3]ClO_4$	−64.6	10l
$[Fe_3O(O_2CCH_3)_6(H_2O)_3]NO_3$	−54	10l
$[NaFe_3O(O_2CPh)_5(pic)_2(EtOH)_2(H_2O)]_2(ClO_4)_2$	−54.8, −41.8	
	−45.4, −63.2	10n

* *J*-values calculated with the $-2J\mathbf{S_iS_j}$ Hamiltonian have been doubled for direct comparison with the ones determined here.